Interaction of Stark-shifted image potential states with quantum well states in ultrathin Ag(111) islands on Si(111)-$\sqrt{3} \times \sqrt{3}$-B substrates

Kishu Sugawara,[1] Kentaro Nagase,[1] Shiro Yamazaki,[1] Kan Nakatsuji,[2] and Hiroyuki Hirayama[1,*]

[1]*Department of Physics, Tokyo Institute of Technology, J1-3, 4259 Nagatsuda, Midori-ku, Yokohama 226-8502, Japan*

[2]*Department of Materials Science and Engineering, Tokyo Institute of Technology, J1-3, 4259 Nagatsuda, Midori-ku, Yokohama 226-8502, Japan*

(Received 22 May 2017; revised manuscript received 10 August 2017; published 30 August 2017)

We studied the thickness-dependent shift of quantum well state (QWS) peaks and their interaction with Stark-shifted image potential states (IPSs) in the dz/dV spectrum of ultrathin Ag(111) islands on a Si(111)-$\sqrt{3} \times \sqrt{3}$-B substrate. The transmission resonance peaks for the QWSs were shifted to lower energy as the Ag island thickness increased. The shift was quantitatively explained by the quantization of the electrons in the island with the specific Γ-L dispersion of Ag. In addition, two split peaks appeared around the original IPS position when the QWS and IPS had the same energy. The split peaks were attributed to the avoidance of the QWS and IPS crossing.

DOI: 10.1103/PhysRevB.96.075444

I. INTRODUCTION

Electrons at surfaces were shown theoretically to be trapped by the image potential to form Rydberg-like bound states on the vacuum side [1,2]. These image potential states (IPSs) have been detected as peaks experimentally by inverse photoemission spectroscopy [3,4] and two-photon photoemission spectroscopy (2PPE) [5]. The electrons in the IPSs were shown experimentally to have free-electron-like parabolic surface dispersion with an effective mass close to the rest mass of an electron, $\sim m_e$ [3,6]. IPSs with free-electron-like dispersion are an ideal simple system for studying the carrier dynamics at surfaces. The lifetime and scattering of the electrons in IPSs have been intensively investigated at several surfaces by time-resolved 2PPE [7–11]. Furthermore, phenomena such as the quantum beat of coherently excited electrons to IPSs [12] and spin-dependent relaxation of IPS electrons on magnetic islands [13] have been investigated using 2PPE in the last decade.

IPSs have been studied by scanning tunneling microscopy (STM). IPSs are Stark shifted by the strong electric field between the tip and sample surface in STM [14]. They manifest themselves as a series of transmission resonance peaks in the field emission regime above the vacuum level in the dz/dV spectrum of STM [15,16]. The peak position of IPSs is sensitive to the work function, and the spatial distribution of the work function can be detected with atomic resolution by STM. The changes in the local work function were detected on various surfaces with nanoislands [17–19], adsorbed molecules [20], and periodic long-range reconstruction by using the shift of the energy position of IPSs in STM [21]. Spatially resolved IPS measurements have also been used to obtain chemical contrasts [22,23] and to determine the local adatom density [24] on surfaces with heterogeneous adatoms. Furthermore, the confinement and scattering of hot electrons in IPSs have been observed experimentally on nanoislands [25,26], stacking fault tetrahedrons [27], and subsurface defects [28]. The dispersion and momentum-resolved phase relaxation time of the first IPS have been measured on the Cu(100) surface by using the quantum interference patterns in STM [29]. The characteristic splitting of the first IPS and its sensitivity to layer-stacking sequences have been demonstrated for monolayer and bilayer graphene on the SiC substrate [30]. The spatial modulation of IPSs has been investigated for single-layer islands and moiré structures of graphene and h-BN on metal substrates [31–33]. Spin-polarized STM has been used to analyze the lifetime of spin-split IPSs on Fe nanomagnets on a W(110) surface [34]. Interaction with periodic surface potential has been reported to split the IPSs at the InAs(111)A surface [35].

In addition to the IPS peaks, weak peaks have been reported to appear in the STM dz/dV spectrum of the ultrathin Ag islands on Si(111)-7 × 7 surfaces [36–38]. These additional peaks are shifted with increasing Ag island thickness. The appearance of the thickness-dependent weak peaks was attributed to simple quantum confinement of free electrons by a particle-in-a-box potential in the Ag island [36–38].

However, the electrons should not be treated as simple free electrons in the Ag island. The motion of the electrons is governed by a specific dispersion relation. The Ag band disperses from the upper edge of the ∼4 eV gap at L to a higher-energy region in the Γ-L orientation (// (111) direction) in the empty state [39–41]. We should consider this specific band dispersion to discuss quantum well states (QWSs) in ultrathin Ag(111) islands [42,43]. Conversely, the Ag thickness-dependent shift of the additional peaks is expected to be useful for determining the dispersion relation experimentally. In this study, we demonstrate that the theoretically calculated empty-state band dispersion [39–41] is experimentally reproduced by the shift of the additional peaks.

Furthermore, we clarify that the interaction of the QWSs with IPSs is observed in the dz/dV spectrum. It has been reported that the IPSs were shifted to higher energy in the dz/dV spectrum by the additional peaks in ultrathin Ag islands on a Si(111)-7 × 7 substrate [36–38]. Similar behavior was also reported in the Si(111)-$\sqrt{3} \times \sqrt{3}$-Sn system [44]. However, the origin of this phenomenon has not been addressed. We reveal that the shift of the IPSs is due to avoiding crossing in the interaction with QWSs when the QWS energy approaches the IPS.

*hirayama.h.aa@m.titech.ac.jp

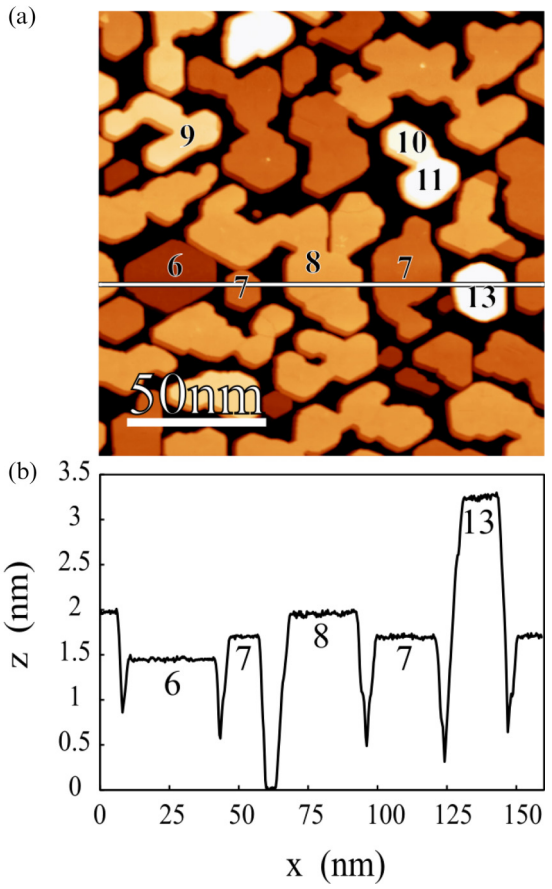

FIG. 1. (a) STM image of Ag islands on a Si(111)-$\sqrt{3} \times \sqrt{3}$-B substrate surface. The numbers indicate the height of the islands as the number of MLs. $V_s = +2.0$ V, $I_t = 0.1$ nA. (b) Cross-sectional profile along the white line in (a).

II. EXPERIMENTS

Experiments were conducted in an ultrahigh-vacuum (UHV) apparatus with a Ag Knudsen cell and a low-temperature STM system [45,46]. The surface of the Si(111)-$\sqrt{3} \times \sqrt{3}$-B substrate was prepared by thermal treatment of a highly boron doped Si(111) wafer ($\rho = 0.09\ \Omega\,\mathrm{cm}^{-3}$). The Si(111) sample was outgassed at 873 K for 10 h by resistive heating in a UHV. The sample was flashed at 1523 K for several seconds and kept for 30 min at 1223 and 1173 K, respectively. A Si(111)-$\sqrt{3} \times \sqrt{3}$-B surface with less than 3% atomic defects was obtained after cooling the sample slowly at a rate of 1.5 K/s. Ag islands were grown by depositing 6.7 monolayers (MLs) of Ag atoms at a rate of 0.67 ML/min on the Si(111)-$\sqrt{3} \times \sqrt{3}$-B surface at room temperature. STM images and dz/dV spectra were taken at the temperature of supercooled liquid nitrogen (65 K). The bias voltage was applied to the sample in the STM. The dz/dV spectra were obtained with a lock-in amplifier at a modulation voltage of 25 meV at 1080 Hz. The feedback loop was kept closed in the dz/dV spectrum measurements.

III. RESULTS AND DISCUSSION

Figure 1(a) shows an STM image of the Ag islands on the Si(111)-$\sqrt{3} \times \sqrt{3}$-B substrate. The islands nucleated directly on the substrate because the dark area between the islands shows the characteristics of the $\sqrt{3} \times \sqrt{3}$ reconstruction of the substrate. The islands were atomically flat, as shown in the cross section in Fig. 1(b). The thicknesses of the islands were multiples of the distance between the Ag(111) planes (0.24 nm), indicating that they were Ag(111) islands. The thicknesses of some islands are shown as the number of Ag(111) MLs in Fig. 1(a). Islands that were 6 to 13 MLs thick nucleated on the substrate after deposition of Ag atoms sufficient to form 6.7 MLs.

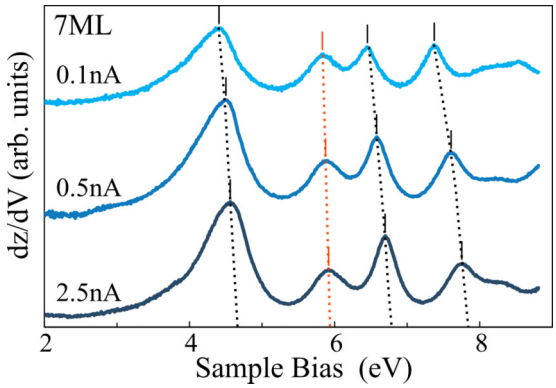

FIG. 2. The dz/dV spectra of a 7-ML-thick Ag(111) island on the Si(111)-$\sqrt{3} \times \sqrt{3}$-B substrate. The $I_t = 0.1$, 0.5, and 2.5 nA spectra are displayed from top to bottom. Peak positions are indicated by short bars. Dotted curves are guides for the eye.

The dz/dV spectrum for a 7-ML-thick Ag island is shown in Fig. 2. Four distinct peaks were observed at 4.4, 5.8, 6.4, and 7.3 eV in the top spectrum, with a tunneling current of $I_t = 0.1$ nA. The peaks at 4.4, 6.4, and 7.3 eV shifted to higher energy when I_t was increased to 0.5 (middle) and 2.5 nA (bottom). The peak at 5.8 eV did not show a major shift with increasing I_t, and its position was almost independent of the increase. The increase in I_t reduces the tip-sample distance and increases the electric field in the confinement potential of IPSs [14]. The IPSs should thus be Stark shifted to higher energies with increasing I_t. Consequently, the three I_t-dependent peaks were assigned as transmission resonance peaks for IPSs. The I_t-dependent shift was larger for the IPS peak at higher energy. This is also reasonable because the Stark shift increases for the IPS at higher energy in the electric-field-induced quasitriangular confinement potential. However, the electrons in the Ag island resided outside of the electric field and were not affected by the change in I_t. Thus, the peak that was not dependent on I_t was assigned as the resonance with the QWS in the Ag island.

The energy positions of the QWSs depended on Ag island thickness. Figure 3 shows the Ag island thickness dependence of the dz/dV spectrum for islands with thicknesses of 4 to 13 MLs. The spectrum of the 11-ML-thick island is not included because it was barely visible by STM. All the spectra were taken at $I_t = 0.1$ nA. We classified the peaks as QWS or IPS by examining the shift with increasing I_t in each spectrum. The QWS peaks are indicated by short bars.

The QWS peaks were shifted to lower energy as the Ag island thickness increased [Fig. 3(a)]. Because the spectra in the figure were taken at the same I_t (0.1 nA), the Stark

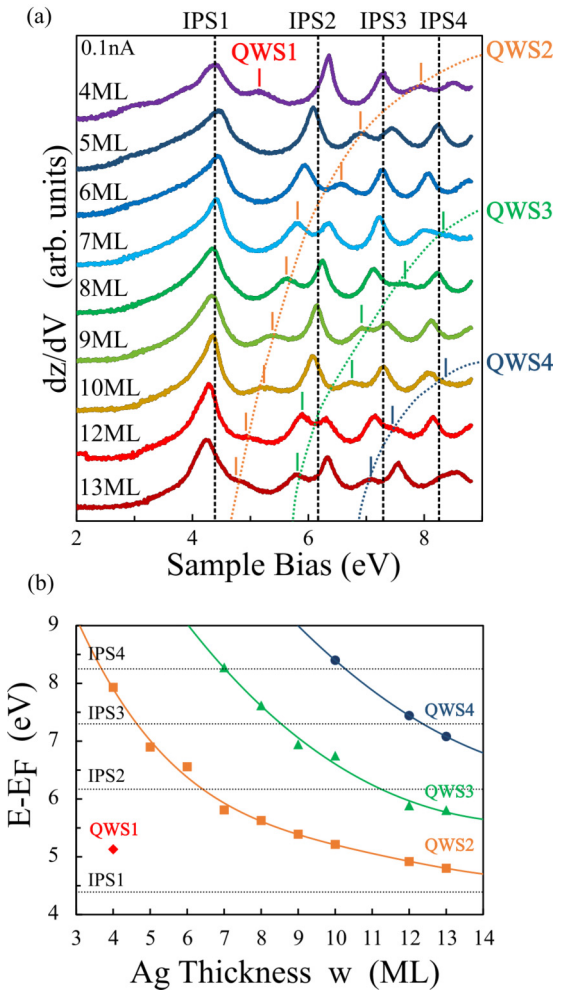

FIG. 3. (a) Dependence on Ag island thickness of the dz/dV spectrum of a Ag(111) ultrathin island on surface of a Si(111)-$\sqrt{3}\times\sqrt{3}$-B substrate. The Ag island thickness is indicated on the left side for each spectrum. The spectra were taken at $I_t = 0.1$ nA. The short bars indicate the QWS peaks that did not show a Stark shift. Dotted curves are guides for the eye. Vertical dotted lines indicate the numerically calculated positions of the first, second, third, and fourth IPS peaks. (b) Relation between Ag island thickness and QWS peak energies. Dots denote experimental data. Solid curves indicate polynomial fitting of the Ag island thickness dependence of the second, third, and fourth QWSs. Dotted horizontal lines indicate numerically calculated energies of the first, second, third, and fourth IPSs.

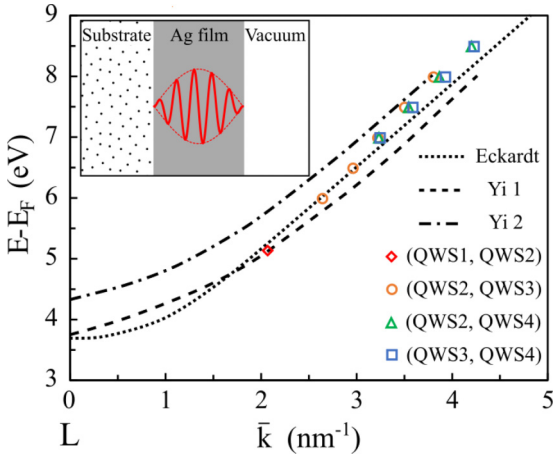

FIG. 4. Comparison of experimentally obtained and theoretically calculated dispersion $E(\bar{k})$ of Ag from the L (left side) to Γ (right side) orientations. Experimental data were obtained from the differences between QWS1 and QWS2 (diamonds), QWS2 and QWS3 (circles), QWS2 and QWS4 (triangles), and QWS3 and QWS4 (squares). The dotted line (Eckardt) is the theoretical dispersion using the Kohn-Sham equation with a local exchange-correlation potential [39,40]. Dashed (Yi 1) and dash-dotted (Yi 2) lines are theoretical dispersions using LDA and the GW approximation [41], respectively. The inset shows a schematic of the wave function of QWS1.

effect did not cause the shift. The peak shift was caused by only the change in the Ag island thickness. The electron band dispersion of Ag extended from the upper edge of the band gap at ~4 eV above the Fermi level to higher energies along the L-Γ direction in the Brillouin zone (curves in Fig. 4) [39–41]. The electrons in this energy range contributed to QWS formation. Wave vector $\bar{k}$ from the L point determined the envelope of the wave function of the confined electron, whereas wave vector k from the Γ point caused oscillation in the envelope in the quantum confinement of the electrons with this dispersion (inset in Fig. 4) [42,43]. $\bar{k}$ and k are functions of energy E in the dispersion relation, and the quantized condition of the electrons is given by the phase accumulation model $2\bar{k}(E)w_n d + \phi_{\rm int}(E) + \phi_{\rm surf}(E) = 2n\pi$. Here, d is the thickness of 1 ML, w_n is the number of MLs in the Ag(111) islands, $\phi_{\rm int}(E)$ and $\phi_{\rm surf}(E)$ are the phase shifts at the interface and surface of the Ag island at energy E, respectively, and n is the quantum number that determines the shape of the envelope function of the confined electrons [47]. The thickness-dependent peaks in Fig. 3(a) were assigned as the n = 1, 2, 3, and 4 QWSs, respectively. Their thickness dependence is plotted by dots along with polynomial fitting curves in Fig. 3(b). The phase shifts $\phi_{\rm int}(E)$ and $\phi_{\rm surf}(E)$ are E dependent and not known, respectively. Therefore, we canceled out the phase shifts by subtracting the phase accumulation models for quantum numbers m and n at the same energy, E, to obtain the equation $2\bar{k}(E)(w_m - w_n)d = 2(m-n)\pi$ [47]. With this equation, we evaluated the relation between $\bar{k}$ and E for $(m,n) = (1,2),(2,3),(2,4)$, and $(3,4)$ at several energies. The experimental results (symbols) were compared with previously reported theoretical dispersions of Ag along the Γ-L direction (curves in Fig. 4). The dotted line represents the theoretical dispersions obtained by solving the relativistic Kohn-Sham equation with a local exchange-correlation potential [39,40]. However, the local-density approximation (LDA) tends to underestimate the band gap. This drawback is improved by the GW approximation. Thus, we reproduced the theoretically calculated dispersion using density-functional theory and the GW approximation by Yi *et al.* [41], as shown by the dashed and dash-dotted lines in Fig. 4. The theoretical dispersions do not agree perfectly. However, the experimental results (symbols) and the theoretically calculated dispersions (curves) [39–41] agreed well on the whole (Fig. 4). Thus, the thickness-dependent peaks were unambiguously assigned as the transmission resonance peaks for the QWSs in the ultrathin

Ag(111) islands. The high-energy empty-state dispersion of ultrathin islands has been detected using the electron reflection with a low-energy electron microscope [48–50]. The present results demonstrate that dz/dV spectroscopy is another useful method for evaluating the high-energy empty-state dispersion relation of ultrathin islands with an atomic spatial resolution.

In contrast to the QWSs, the IPS peaks did not shift with changing Ag island thickness. However, the IPS peaks were slightly shifted to reveal two split peaks when the QWS peaks approached their original position. The split peaks occurred at the crossing point of 7 MLs for IPS2 and QWS2, about 9 MLs for IPS3 and QWS3, and 12–13 MLs for IPS2 and QWS3 in Fig. 3(a). For IPS2, IPS3, and IPS4, the IPS peak was shifted to lower energy when the QWS peak approached from higher energy, whereas it was shifted to higher energy when QWS shifted to lower energy in the continuous shift of the QWS peaks.

This behavior was not observed for IPS1. IPS1 showed a gradual shift to lower energy from 4 to about 9 MLs. This may have resulted from a change in the spectral weight caused by the approaching QWS1. However, no split peaks occurred at larger heights for IPS1 because IPS1 was almost at the vacuum level. The Ag(111) surface has a work function of 4.46 eV [51]. The transmission resonance does not occur for peaks at an energy below the vacuum level. Thus, the peak would hardly be visible below the transmission resonance energy if the shift and split occurred for IPS1.

To understand the shift around the intersection, we numerically evaluated the intrinsic energy positions of the IPSs. Figure 5(a) shows the model potential for the numerical calculation of IPSs. We used the sum of the image potential at the Ag island surface (green dashed line) and the tip-sample electric field potential (blue dashed line) as the total potential (red solid line) that binds the IPSs. The electric field potential was determined by the bias voltage V_s over the tip-sample distance. In dz/dV spectroscopy, the tip-surface distance is increased stepwise when V_s coincides with the bound state and a new transmission resonant channel is opened. The absolute tip-surface distance was defined by adding an offset to the experimentally observed relative z increment of the STM tip position. The Ag surface was assumed to be an infinite potential wall. The Schottky effect [52] at the tip surface was neglected for simplicity. The energy levels of the bound states E_B were obtained by numerically solving the Shrödinger equation under the quasitriangular potentials as a function of V_s. The IPS transmission resonance peak in the spectrum was determined as the specific V_s (Fermi level of the tip), which coincided with E_B. The initial offset of the tip-surface distance was chosen to reproduce the experimentally observed IPS3 (7.30 eV) for the 10-ML-thick Ag(111) island in the calculation because IPS3 was separate enough from the adjacent QWS peaks at 10 MLs to suppress their extrinsic effect on the energy position of IPS3. The calculated energies of the IPS peak positions are shown in Fig. 5(b). The calculation reproduced the experimentally observed transmission resonances with the first, second, and fourth IPSs satisfactorily.

The IPSs and QWSs are spatially aligned in series along the surface-normal orientation and are recognized as a double-quantum-well system. The unusual shift of the IPSs and QWSs

(a)

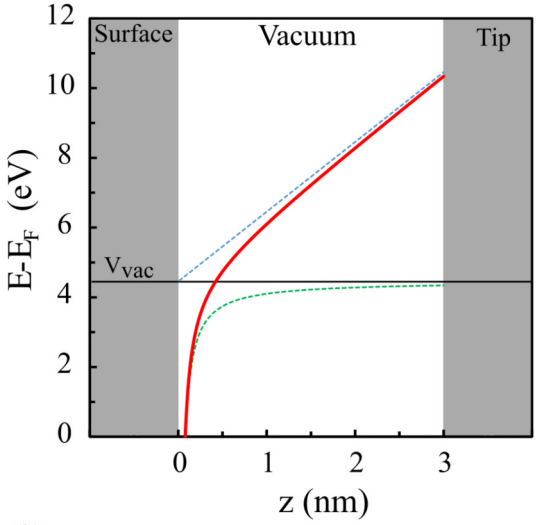

(b)

	model (eV)	Experiment (eV)
IPS1	4.39	4.34
IPS2	6.17	6.08
IPS3	7.30	7.30
IPS4	8.25	8.08

FIG. 5. (a) Model potential for the numerical calculation of IPSs. The image potential at the Ag island surface and tip-surface electric field potential are indicated by green and blue dashed lines, respectively. The total potential on the vacuum side (red solid line) is given by the sum of these two potentials. Distance from the Ag island surface is indicated on the horizontal axis in nanometers. The tip-surface distance is 3.0 nm, and the bias voltage is $V_s = 6.0$ eV. IPSs are calculated as the bound states between the surface and the red solid line potential on the vacuum side. (b) Comparison of the numerically calculated energies of the IPSs and experimental values.

around their intersections is the avoided crossing [53,54] between the two bound states in the double quantum well. In the simplest picture, the system is described by the following Hamiltonian:

$$H = \begin{pmatrix} H_{\mathrm{IPS}} & H' \\ H'^{*} & H_{\mathrm{QWS}} \end{pmatrix}. \tag{1}$$

Here, H_{IPS} and H_{QWS} are the noninteracting Hamiltonians with eigenenergies E_{IPS} and E_{QWS} for the IPSs and QWSs, respectively. H' describes the interaction between IPS and QWS. The eigenstates of this Hamiltonian are given by

$$E = \frac{(E_{\mathrm{IPS}} + E_{\mathrm{QWS}}) \pm \sqrt{(E_{\mathrm{IPS}} - E_{\mathrm{QWS}})^2 + 4V_{\mathrm{int}}^2}}{2}, \tag{2}$$

where $V_{\mathrm{int}} = \langle \mathrm{IPS} \mid H' \mid \mathrm{QWS} \rangle$ is the amplitude of the interaction between IPS and QWS. The equation predicts that the two states split by $\pm V_{\mathrm{int}}$ from their nonperturbed energy, $(E_{\mathrm{IPS}} + E_{\mathrm{QWS}})/2$, when E_{IPS} is close enough to E_{QWS} (i.e.,

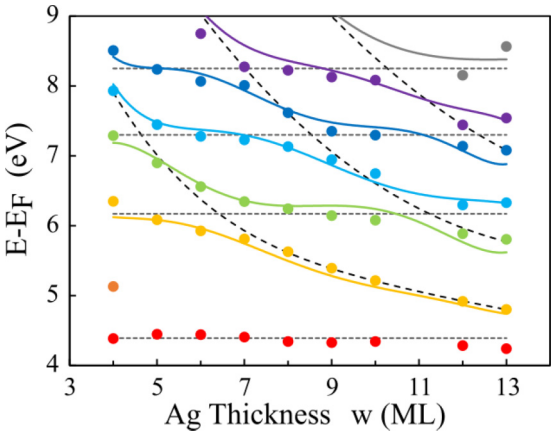

FIG. 6. Numerically calculated avoided crossing and experimental data. Solid curves show interpolation of numerically calculated peak positions with the avoided crossing with $V_{int} = 0.3$ eV. Solid circles denote experimentally observed peak positions in Fig. 3(a). Horizontal dashed lines indicate calculated energy positions of IPSs shown in Fig. 5(b). Dashed curves indicate polynomial fittings of the dependence on Ag island thickness of the QWS peaks shown in Fig. 3(b).

$E_{IPS} \sim E_{QWS}$). E approaches the intrinsic energies of IPS (E_{IPS}) and QWS (E_{QWS}) when E_{QWS} is far from E_{IPS} (i.e., $|E_{IPS} - E_{QWS}| \gg V$). Equation (2) explains the specific shift of the peaks around the intersection of the IPSs and QWSs in Fig. 3(a). Quantitatively, two peaks were separated by ± 0.3 eV at the intersection between IPS2 and QWS1 at 7 MLs and IPS2 and QWS2 at 12 MLs in the experiment. Therefore, we assumed $V_{int} = 0.3$ eV. Then, we calculated E in Eq. (2) for all the intersections between noninteracting E_{IPS} and E_{QWS}. We used the calculated energy in Fig. 5(b) and the polynomial fitting curves of the experimental data in Fig. 3(b) for E_{IPS} and E_{QWS}, respectively. E_{IPS} and E_{QWS} are indicated by horizontal dashed lines and dashed curves, respectively, in Fig. 6. E calculated by Eq. (2) at each ML thickness and interpolated is shown by the solid curves. Solid circles represent the experimentally observed peak positions of IPSs and QWSs. The calculation reproduced the experimentally observed peak positions satisfactorily. Thus, the avoided crossing caused the unusual shift of the IPSs and QWSs around the intersections.

The control of the two QWSs in the double quantum well is an intriguing topic in the implementation of quantum bits [55]. In the coupled-quantum-dot molecular system, an electric field is applied to the buried coupled dots in semiconductors [56]. However, the electric field shifts the two QWSs in this system. In contrast, the present system allows for control of the two QWSs independently. The IPS is controlled by the electric field via the tip-surface distance, whereas the QWS is shifted by the Ag island thickness. We suggest that the present system is unique and advantageous for investigating the control of the two QWSs in a double quantum well.

IV. SUMMARY

We conducted dz/dV spectroscopy for ultrathin Ag(111) islands on the surface of a Si(111)-$\sqrt{3} \times \sqrt{3}$-B substrate. The transmission resonances with the IPSs and QWSs in the ultrathin Ag islands were observed as peaks in the spectrum. The IPSs showed a Stark shift as the tip-surface distance changed, whereas QWSs were shifted as the Ag island thickness increased. The IPS peaks were satisfactorily reproduced by numerically solving the Shrödinger equation under the image potential at the surface side and the electric field. The thickness dependence of the QWS peaks experimentally reproduced the theoretically calculated band dispersion of Ag along the Γ-L direction in the high-energy empty state. Furthermore, the IPSs showed a characteristic shift when the energies of the QWS and IPS aligned. This observation was explained quantitatively by the avoidance of crossing between the IPS and QWS.

ACKNOWLEDGMENT

This work was supported by JSPS KAKENHI Grant No. 6286048.

[1] P. M. Echenique and J. Pendry, J. Phys. C **11**, 2065 (1978).
[2] E. V. Chulkov, V. M. Silkin, and P. M. Echenique, Surf. Sci. **437**, 330 (1999).
[3] A. Goldmann, V. Dose, and G. Borstel, Phys. Rev. B **32**, 1971 (1985).
[4] F. J. Himpsel and J. E. Ortega, Phys. Rev. B **46**, 9719 (1992).
[5] K. Giesen, F. Hage, F. J. Himpsel, H. J. Riess, and W. Steinmann, Phys. Rev. Lett. **55**, 300 (1985).
[6] K. Giesen, F. Hage, F. J. Himpsel, H. J. Riess, W. Steinmann, and N. V. Smith, Phys. Rev. B **35**, 975 (1987).
[7] M. Weinelt, J. Phys. Condens. Matter **14**, R1099 (2002).
[8] Th. Fauster, C. Reuß, I. L. Shumay, and M. Weinelt, Chem. Phys. **251**, 111 (2000).
[9] S. S. Tsirkin, S. V. Eremeev, E. V. Chulkov, M. Marks, K. Schubert, J. Güdde, and U. Höfer, Phys. Rev. B **86**, 085424 (2012).
[10] K. Schubert, A. Damm, S. V. Eremeev, M. Marks, M. Shibuta, W. Berthold, J. Güdde, A. G. Borisov, S. S. Tsirkin, E. V. Chulkov, and U. Höfer, Phys. Rev. B **85**, 205431 (2012).
[11] I. L. Shumay, U. Höfer, Ch. Reuß, U. Thomann, W. Wallauer, and Th. Fauster, Phys. Rev. B **58**, 13974 (1998).
[12] M. Marks, C. H. Schwalb, K. Schubert, J. Güdde, and U. Höfer, Phys. Rev. B **84**, 245402 (2011).
[13] A. B. Schmidt, M. Pickel, M. Donath, P. Buczek, A. Ernst, V. P. Zhukov, P. M. Echenique, L. M. Sandratskii, E. V. Chulkov, and M. Weinelt, Phys. Rev. Lett. **105**, 197401 (2010).
[14] D. B. Dougherty, P. Maksymovych, J. Lee, M. Feng, H. Petek, and J. T. Yates, Jr., Phys. Rev. B **76**, 125428 (2007).
[15] G. Binnig, K. H. Frank, H. Fuchs, N. Garcia, B. Reihl, H. Rohrer, F. Salvan, and A. R. Williams, Phys. Rev. Lett. **55**, 991 (1985).
[16] R. S. Becker, J. A. Golovchenko, and B. S. Swartzentruber, Phys. Rev. Lett. **55**, 987 (1985).

[17] M. Pivetta, F. Patthey, M. Stengel, A. Baldereschi, and W.-D. Schneider, Phys. Rev. B **72**, 115404 (2005).
[18] H-C. Ploigt, C. Brun, M. Pivetta, F. Patthey, and W.-D. Schneider, Phys. Rev. B **76**, 195404 (2007).
[19] P. Ruffieux, K. Aït-Mansour, A. Bendounan, R. Fasel, L. Patthey, P. Gröning, and O. Gröning, Phys. Rev. Lett. **102**, 086807 (2009).
[20] D. B. Dougherty, P. Maksymovych, J. Lee, and J. T. Yates, Jr., Phys. Rev. Lett. **97**, 236806 (2006).
[21] S. Polei, I. Barke, S. C. Erwin, and K.-H. Meiwes-Broer, Phys. Rev. B **85**, 165414 (2012).
[22] T. Jung, Y. W. Mo, and F. J. Himpsel, Phys. Rev. Lett. **74**, 1641 (1995).
[23] J. Mysliveček, F. Dvořák, A. Stróżecka, and B. Voigtländer, Phys. Rev. B **81**, 245427 (2010).
[24] C. Zaum, J. Meyer, K. Reuter, and K. Morgenstern, Phys. Rev. B **90**, 165418 (2014).
[25] K. Schouteden and C. Van Haesendonck, Phys. Rev. Lett. **103**, 266805 (2009).
[26] S. Stepanow, A. Mugarza, G. Ceballos, P. Gambardella, I. Aldazabal, A. G. Borisov, and A. Arnau, Phys. Rev. B **83**, 115101 (2011).
[27] K. Schouteden and C. Van Haesendonck, Phys. Rev. Lett. **108**, 076806 (2012).
[28] J. I. Pascual, C. Corriol, G. Ceballos, I. Aldazabal, H.-P. Rust, K. Horn, J. M. Pitarke, P. M. Echenique, and A. Arnau, Phys. Rev. B **75**, 165326 (2007).
[29] P. Wahl, M. A. Schneider, L. Diekhöner, R. Vogelgesang, and K. Kern, Phys. Rev. Lett. **91**, 106802 (2003).
[30] S. Bose, V. M. Silkin, R. Ohmann, I. Brihuega, L. Vitali, C. M. Michaelis, P. Mallet, J. Y. Veuillen, M. A. Schneider, E. V. Chulkov, P. M. Echenique, and K. Kern, New J. Phys. **12**, 023028 (2010).
[31] F. Craes, S. Runte, J. Klinkhammer, M. Kralj, T. Michely, and C. Busse, Phys. Rev. Lett. **111**, 056804 (2013).
[32] B. Borca, S. Barja, M. Garnica, D. Sánchez-Portal, V. M. Silkin, E. V. Chulkov, C. F. Hermanns, J. J. Hinarejos, A. L. Vázquez de Parga, A. Arnau, P. M. Echenique, and R. Miranda, Phys. Rev. Lett. **105**, 036804 (2010).
[33] S. Joshi, D. Ecija, R. Koitz, M. Iannuzzi, A. P. Seitsonen, J. Hutter, H. Sachdev, S. Vijayaraghavan, F. Bischoff, K. Seufert, J. V. Barth, and W. Auwärter, Nano Lett. **12**, 5821 (2012).
[34] A. Schlenhoff, S. Krause, A. Sonntag, and R. Wiesendanger, Phys. Rev. Lett. **109**, 097602 (2012).
[35] J. Martínez-Blanco, S. C. Erwin, K. Kanisawa, and S. Fölsch, Phys. Rev. B **92**, 115444 (2015).
[36] W. B. Su, S. M. Lu, H. T. Shih, C. L. Jiang, C. S. Chang, and T. T. Tsong, J. Phys. Condens. Matter. **18**, 6299 (2006).
[37] W. B. Su, S. M. Lu, C. L. Jiang, H. T. Shih, C. S. Chang, and T. T. Tsong, Phys. Rev. B **74**, 155330 (2006).
[38] S.-M. Lu, H.-H. Huang, W.-B. Su, P.-H. Chu, C.-S. Chang, H.-L. Hsiao, and T.-T. Tsong, Jpn. J. Appl. Phys. **50**, 08LB01 (2011).
[39] S. C. Wu, H. Li, J. Sokolov, J. Quinn, Y. S. Li, and F. Jona, J. Phys. Condens. Matter **1**, 7471 (1989).
[40] H. Eckardt, L. Fritsche, and J. Noffke, J. Phys. F **14**, 97 (1984).
[41] Z. Yi, Y. Ma, M. Rohlfing, V. M. Silkin, and E. V. Chulkov, Phys. Rev. B **81**, 125125 (2010).
[42] T.-C. Chiang, Surf. Sci. Rep. **39**, 181 (2000).
[43] M. Watai and H. Hirayama, Phys. Rev. B **72**, 085435 (2005).
[44] J. A. Kubby, Y. R. Wang, and W. J. Greene, Phys. Rev. Lett. **65**, 2165 (1990).
[45] K. Sawa, Y. Aoki, and H. Hirayama, Phys. Rev. B **80**, 035428 (2009).
[46] K. Sawa, Y. Aoki, and H. Hirayama, Phys. Rev. Lett. **104**, 016806 (2010).
[47] I. Matsuda, H. W. Yeom, T. Tanikawa, K. Tono, T. Nagao, S. Hasegawa, and T. Ohta, Phys. Rev. B **63**, 125325 (2001).
[48] K. L. Man, Z. Q. Qiu, and M. S. Altman, Phys. Rev. B **81**, 045426 (2010).
[49] S. Egger, C. H. Back, J. Krewer, and D. Pescia, Phys. Rev. Lett. **83**, 2833 (1999).
[50] Q. Wu and M. S. Altman, Ultramicroscopy **130**, 109 (2013).
[51] M. Chelvayohan and C. Mee, J. Phys. C **15**, 2305 (1982).
[52] S. M. Sze, *Physics of Semiconductor Devices* (Wiley, New York, 1981).
[53] L. D. Landau and L. M. Lifshitz, *Quantum Mechanics* (Butterworth-Heinemann, Amsterdam, 1981).
[54] I. Lizuain, E. Hernández-Concepción, and J. G. Muga, Phys. Rev. A **79**, 065602 (2009).
[55] E. Biolatti, R. C. Iotti, P. Zanardi, and F. Rossi, Phys. Rev. Lett. **85**, 5647 (2000).
[56] H. J. Krenner, M. Sabathil, E. C. Clark, A. Kress, D. Schuh, M. Bichler, G. Abstreiter, and J. J. Finley, Phys. Rev. Lett. **94**, 057402 (2005).